

NATURAL CONVECTION ANALYSIS IN VERTICAL UPRIGHT-ANGLED TRIANGULAR CAVITIES WITH UNIFORMLY HEATED VERTICAL WALL AND ISOTHERMALLY COOLED HYPOTENUSE

Martínez-Suárez J.A.^a, Sieres J.^{a*}, Campo A.^b

^aÁrea de Máquinas y Motores Térmicos, Escuela de Ingeniería Industrial, Campus Universitario Lagoas-
Marcosende, University of Vigo, 36310 Vigo, Spain

^bThe University of Texas at San Antonio, Department of Mechanical Engineering, San Antonio, TX 78249, USA

* Author for correspondence: E-mail: jsieres@uvigo.es, Tel: +34 986 811997, Fax: +34 986 811995

ABSTRACT

Steady-state laminar natural convection in triangular enclosures is of interest in many engineering applications such as buildings and electronic equipment.

This paper presents an analytical and numerical computation of laminar natural convection in vertical upright-angled triangular cavities filled with air. The vertical wall is uniformly heated; a prescribed cold temperature is assigned at the inclined wall; while the upper horizontal wall is assumed thermally insulated. The defining aperture angle φ is located at the lower vertex between the vertical and inclined walls.

The finite element method is implemented to perform the computational analysis for three aperture angles φ ($= 15^\circ, 30^\circ$ and 45°) and height-based Rayleigh numbers ranging from a low $Ra = 0$ (pure conduction) to a high 10^9 . Numerical results are reported for the buoyant velocity and temperature fields as well as the mean convective coefficient at the heated vertical wall. The numerical computations are also focused on the determination of the value of the maximum or critical temperature along the hot vertical wall.

NOMENCLATURE

g	[m/s ²]	Gravitational acceleration
k	[W/mK]	Thermal conductivity
L	[m]	Length of wall
Nu	[-]	Nusselt number, $Nu = q_H L_H / (k (T - T_C))$
Nu_1	[-]	Minimum Nusselt number along the hot wall
Nu_2	[-]	Mean Nusselt number along the hot wall
p	[Pa]	Pressure
P	[-]	Dimensionless pressure, $p / (\rho \cdot V_c^2)$
Pr	[-]	Prandtl number
q	[W/m ²]	Heat flux
Ra	[-]	Modified Rayleigh number, $Ra = g \cdot q_H \cdot L_H^4 / (\alpha \cdot \nu \cdot k \cdot T_C)$
s	[m]	Distance along the wall
T	[K]	Absolute temperature
u	[m/s]	Velocity
U	[-]	Dimensionless velocity, $U = u / V_c$

V_c	[m/s]	Characteristic velocity
x, y	[m]	Cartesian coordinates
X, Y	[-]	Dimensionless Cartesian coordinates

Greek symbols		
α	[m ² /s]	Thermal diffusivity
β	[1/K]	Coefficient of volumetric thermal expansion
ΔT	[K]	Temperature differences in the fluid
θ	[-]	Dimensionless temperature, $k \cdot (T - T_C) / (q_H \cdot L_H)$
μ	[kg/ms]	Dynamic viscosity
ν	[m ² /s]	Kinematic viscosity
ρ	[kg/m ³]	Density
φ	[rad]	Aperture angle

Subscripts	
A	Adiabatic
C	Cold
H	Hot
x, y	Components in the x and y directions
X, Y	Components in the dimensionless X and Y directions

INTRODUCTION

Natural convection in enclosures is encountered in many engineering applications. Because of this, it has become an important area for theoretical, computational and experimental research resulting in a vast number of publications in mainstream journals. Typical applications, such as natural convection in house attics, solar collectors, double-pane windows and electronic equipment can be mentioned.

There are many theoretical, numerical and experimental studies in the open literature concerning natural convection in two dimensional enclosures of square, rectangular and triangular cross sections. State-of-the-art reviews of natural convection in enclosures were published by Ostrach [1], Raithby and Hollands [2] and Jaluria [3] in chapters of specialized handbooks. Most of the studies are devoted to natural convection in enclosures with different thermal boundary conditions either for laminar or turbulent regimes [4-9].

Though different thermal boundary conditions have been studied, most papers are focused on the consideration of prescribed uniform temperatures at selected walls of the cavity. Usually, one of the walls is modeled as a hot wall with uniform temperature, a second one is the cold wall also with uniform temperature and the remaining walls are assumed to be thermally insulated. However, in some cases, as found in cooling of electronic components, a more realistic analysis would be obtained if the hot wall is modeled as a uniformly heated wall. Obviously, in these situations an uneven temperature profile is obtained along the hot wall. Knowledge of the value and location of the maximum or critical temperature along the hot vertical is crucial for a correct design of the heat rejection mechanism of these components.

This paper addresses the analytical and numerical computation of laminar natural convection in vertical upright-angled triangular cavities filled with air. This configuration may find application in the miniaturization of electronic packaging subjected to space and/or weight constraints, as stated by Simons et al. [10] and Bar-Cohen et al. [11].

In this work, the vertical wall is uniformly heated; a prescribed cold temperature is assigned at the inclined wall; while the upper horizontal wall is assumed thermally insulated. The numerical computations are obtained with the implementation of the finite element method in a suitable computational grid. Numerical results are obtained for the velocity and temperature fields as well as the Nusselt number at the heated vertical wall for different values of the height-based Rayleigh number. Two different Nusselt numbers are determined: the first is based on the maximum temperature along the heated vertical wall, whereas the second one is based on the mean temperature along the vertical wall. Knowledge of the Nusselt as a function of the Rayleigh number will allow estimating the maximum or critical temperature along the hot vertical wall.

PHYSICAL SYSTEM AND MATHEMATICAL MODEL

The physical system considered in the paper is depicted in Figure 1. It consists of air confined to a vertically-oriented right-angled triangular cavity made with three impermeable walls. The aperture angle φ identifies the bottom vertex of the triangular cavity. A uniform heat flux q_H is imposed at the vertical wall of length L_H , the inclined wall of length L_C is maintained at a uniform cold temperature T_C ; while the upper connecting horizontal wall of length L_A is considered to be thermally insulated.

Owing that the dimension perpendicular to the plane of the diagram is long compared to the cavity height, the air motion is conceived to be two-dimensional. Because the gravitational acceleration g acts parallel to the hot vertical wall, the buoyant air convection may be modeled by the following system of steady conservation equations:

Mass conservation:

$$\frac{\partial u_x}{\partial x} + \frac{\partial u_y}{\partial y} = 0 \quad (1)$$

Momentum equations:

$$\rho \cdot u_x \cdot \frac{\partial u_x}{\partial x} + \rho \cdot u_y \cdot \frac{\partial u_x}{\partial y} = -\frac{\partial p}{\partial x} + \mu \cdot \frac{\partial^2 u_x}{\partial x^2} + \mu \cdot \frac{\partial^2 u_x}{\partial y^2} \quad (2)$$

$$\rho \cdot u_x \cdot \frac{\partial u_y}{\partial x} + \rho \cdot u_y \cdot \frac{\partial u_y}{\partial y} = -\frac{\partial p}{\partial y} + \mu \cdot \frac{\partial^2 u_y}{\partial x^2} + \mu \cdot \frac{\partial^2 u_y}{\partial y^2} - \rho \cdot g \cdot \beta \cdot (T - T_C) \quad (3)$$

Energy conservation:

$$u_x \cdot \frac{\partial T}{\partial x} + u_y \cdot \frac{\partial T}{\partial y} = \alpha \cdot \frac{\partial^2 T}{\partial x^2} + \alpha \cdot \frac{\partial^2 T}{\partial y^2} \quad (4)$$

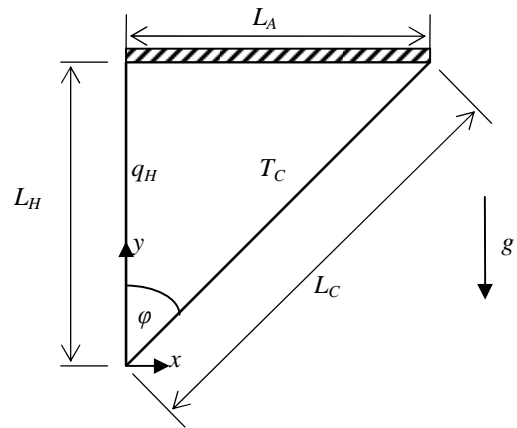


Figure 1 Sketch of the upright-angled triangular cavity.

The Boussinesq approximation and constant physical properties are considered in the previous equations, where ρ denotes a reference density evaluated at the temperature of the cold wall (T_C).

Assuming that the trapped air does not slip at the cavity walls, the velocity boundary conditions are $u_x = u_y = 0$. The temperature boundary conditions refer to a prescribed low temperature T_C at the inclined wall and a uniform heat flux (q_H) at the vertical wall. At the top horizontal wall, the heat flux must be zero to comply with a thermally insulated condition, which implies $\partial T / \partial y = 0$.

For convenience, the governing equations are expressed in terms of suitable dimensionless variables. In order to do this, it is necessary to introduce a characteristic velocity. This characteristic velocity can be obtained from the kinetic energy gained by the fluid as a result of the work done by the buoyancy forces. A measure of the buoyancy forces per unit volume within the cavity is given by $g \cdot \beta \cdot \rho \cdot \Delta T$, where ΔT is a measure of the temperature changes existing in the fluid. The buoyancy forces do work on the fluid as it flows inside the cavity; therefore, a measure of the work done on the fluid can be obtained as the product of the buoyancy forces and a measure of the distance over which these forces act; i.e. a characteristic size of the cavity. In this paper, the cavity height, L_H , is considered as the characteristic size of the cavity. Then, equating the measures of the work done by the buoyancy forces and the kinetic energy gained by the fluid, gives:

$$g \cdot \beta \cdot \rho \cdot \Delta T \cdot L_H = \frac{1}{2} \cdot \rho \cdot V_c^2 \quad (5)$$

Most natural convection problems can be included in one of the following two categories:

- External flow configurations where the surface temperature (T_w) and ambient temperature (T_∞) are given as input parameters. In these cases a measure of the temperature changes existing in the flow is simply given by $\Delta T = T_w - T_\infty$.

- Internal flow configurations that occur within enclosed regions where prescribed uniform hot (T_H) and cold (T_C) temperatures are specified along some of its walls. Then, a measure of the temperature changes in the flow is given by $\Delta T = T_H - T_C$.

In the problem considered in this paper, a prescribed uniform cold temperature (T_C) is considered along the inclined wall and a uniform heat flux (q_H) is considered along the vertical wall. In this case, the vertical wall temperature increases with height, and is expected to reach a maximum at the upper edge of the wall. In order to obtain a measure of the temperature changes in the flow, the heat flux at the vertical wall is related with fluid temperature field by virtue of the Fourier's law:

$$q_H = -k \cdot \frac{\partial T}{\partial x} \quad (6)$$

The order of the temperature gradient within the fluid along the vertical coordinate is given by:

$$\frac{\partial T}{\partial x} \sim \frac{T_C - T_w}{L_y} \quad (7)$$

where T_w is the temperature of the vertical wall at the vertical position y and L_y is the horizontal distance from the vertical wall to the inclined wall at position y . As a result, the temperature along the vertical wall is supposed to increase with the vertical position, with a maximum located at the upper corner of the cavity. Then, the order of the temperature changes existing in the flow is given by:

$$\Delta T = T_{w,\max} - T_C \sim \frac{q_H \cdot L_A}{k} \quad (8)$$

Combining Eqs. (6) to (8) and taking into account that $L_A \sim L_H$, the value of the characteristic velocity of the flow is obtained:

$$V_c = \sqrt{\frac{2 \cdot g \cdot \beta \cdot q_H \cdot L_H \cdot L_A}{k}} \quad (9)$$

For convenience, we drop the factor 2 from the square root and replace $L_A \sim L_H$, to obtain the following expression for the characteristic velocity:

$$V_c = \sqrt{\frac{g \cdot \beta \cdot q_H \cdot L_H^2}{k}} \quad (10)$$

The governing equations can also be nondimensionalized by employing the characteristic velocity (V_c) for the flow and the following dimensionless variables:

$$X = \frac{x}{L_H}, Y = \frac{y}{L_H} \quad (11)$$

$$U_X = \frac{u_x}{V_c}, U_Y = \frac{u_y}{V_c} \quad (12)$$

$$\theta = \frac{T - T_C}{\Delta T} = k \cdot \frac{T - T_C}{q_H \cdot L_H}, P = \frac{p}{\rho \cdot V_c^2} \quad (13)$$

Then,

$$V_c = \sqrt{\frac{g \cdot \beta \cdot q_H \cdot L_H^2}{k}} = \sqrt{\frac{g \cdot q_H \cdot L_H^2}{T_C \cdot k}} \quad (14)$$

Resulting:

$$\frac{\partial U_X}{\partial X} + \frac{\partial U_Y}{\partial Y} = 0 \quad (15)$$

$$U_X \cdot \frac{\partial U_X}{\partial X} + U_Y \cdot \frac{\partial U_X}{\partial Y} = -\frac{\partial P}{\partial X} + \frac{\sqrt{Pr}}{\sqrt{Ra}} \left(\frac{\partial^2 U_X}{\partial X^2} + \frac{\partial^2 U_X}{\partial Y^2} \right) \quad (16)$$

$$U_X \cdot \frac{\partial U_Y}{\partial X} + U_Y \cdot \frac{\partial U_Y}{\partial Y} = -\frac{\partial P}{\partial Y} + \frac{\sqrt{Pr}}{\sqrt{Ra}} \left(\frac{\partial^2 U_Y}{\partial X^2} + \frac{\partial^2 U_Y}{\partial Y^2} \right) - \theta \quad (17)$$

$$U_X \cdot \frac{\partial \theta}{\partial X} + U_Y \cdot \frac{\partial \theta}{\partial Y} = \frac{1}{\sqrt{Pr \cdot Ra}} \left(\frac{\partial^2 \theta}{\partial X^2} + \frac{\partial^2 \theta}{\partial Y^2} \right) \quad (18)$$

In the previous equations it has been considered that ($\beta = 1/T_C$):

$$Ra = \frac{g \cdot \beta \cdot \Delta T \cdot L_H^3}{\nu \cdot \alpha} = \frac{g \cdot q_H \cdot L_H^4}{T_C \cdot k \cdot \nu \cdot \alpha} \quad (19)$$

The velocity boundary conditions for the dimensionless governing equations are $U_X = U_Y = 0$. The temperature boundary conditions are established by specifying prescribed values of $\theta = 0$ at the inclined wall, $\partial \theta / \partial X = -1$ at the vertical wall and $\partial \theta / \partial Y = 0$ at the top adiabatic wall.

From the previous set of equations, it is seen that the flow field (U_X, U_Y) and the temperature distribution (θ) are governed, for a given aperture angle (φ), by the Rayleigh number and the Prandtl number.

The governing equations and boundary conditions were solved numerically using the commercial finite element code, COMSOL Multiphysics version 3.5 [12]. The problem was solved using the numerical solver UMFPAK [13]. Computational meshes consisting of roughly 2,400, 6,300 and 10,300 triangular elements were used to make a decision on the grid size. In all cases care was taken to increase the element density in vulnerable areas where high velocity and temperature gradients would occur, such as near the solid walls.

Table 1 shows the results of the grid sensitivity analysis for a critical case corresponding to the widest aperture angle ($\varphi = 45^\circ$) and the highest $Ra = 10^9$. Important parameters such as the maximum nondimensional velocity and temperature values and

the Nusselt numbers at the hot wall are reported. It can be seen that results reported in Table 1 are similar and no appreciable differences (lower than 0.1%) are found when increasing the grid size from 6,300 to 10,300. As a result, in this work a mesh consisting of roughly 6,300 triangular elements was chosen to carry out the entire numerical computations.

Table 1
Grid sensitivity for $Ra = 10^9$ and $\phi = 45^\circ$.

Mesh	U_{max}	Nu_1	Nu_2
2404	$4.44 \cdot 10^{-2}$	14.89	29.32
6304	$4.32 \cdot 10^{-2}$	14.86	29.33
10334	$4.32 \cdot 10^{-2}$	14.86	29.33

RESULTS AND DISCUSSION

Results are reported for the velocity (U_x, U_y) and temperature θ fields as well as the Nusselt numbers at the hot wall, based on the maximum and average hot wall temperature. In this paper, numerical results are reported for three different aperture angles $\phi = 15^\circ, 30^\circ$ and 45° and height-base Rayleigh numbers that range from a low $Ra = 0$ (pure conduction) to a high $Ra = 10^9$. All computations were performed at standard atmospheric pressure. The cold wall temperature T_C and the heat uniform heat flux along the hot wall q_H were set to fixed values of 287 K and 20 W/m^2 , respectively. Perfect gas behavior was assumed, so the thermal expansion coefficient β is given by $1/T_C$. The thermophysical properties of air were assumed constant and evaluated at the cold wall temperature T_C using the code REFPROP [14]. Consequently, all the numerical computations share a same Prandtl number, so for a given aperture angle (ϕ) the velocity and temperature fields are only governed by the Rayleigh number.

Since for all geometries, fixed values of the heat flux and cold wall temperature are considered, the Rayleigh number was controlled through the variation of the gravitational constant g . In particular, the case for $g = 0$ corresponds to the limiting conduction regime, $Ra = 0$.

Figure 2 shows the nondimensional velocity and temperature contours of the air flow for the 45° cavity and a low $Ra = 10^3$. The figure shows that the velocity field for this configuration contains a single clockwise rotating vortex, which takes the shape of the cavity. The vortex moves the warm fluid from the left vertical wall along the top of the cavity and then down along the adiabatic inclined wall. It is also seen that the velocity field is zero at the boundary walls.

With respect to the temperature field, it can be seen that the main orientation of the temperature isotherms is vertical which denotes that, for this low Rayleigh number, the process is dominated by conduction. The maximum temperature is obtained at the upper edge of the hot vertical wall, with a value of $\theta_{max} = 0.508$. This trend should be expected, since the separation between the heated wall and the cold wall grows from the bottom to the top of the cavity gradually. It can also be observed that the isotherms are normal to the top wall, in harmony with the imposed adiabatic boundary condition.

The same results for the slender 15° cavity are shown in Figure 3. Once again a single clockwise rotating vortex is obtained, which is qualitatively similar to the case of the 45° cavity. However, two main differences are appreciated with respect to the 45° cavity: the velocity values are lower (now $U_{max} = 2.61 \cdot 10^{-3}$) and the vortex has moved up towards the top-left-corner of the cavity. As a result, a similar temperature field is expected, which is confirmed in the isotherms represented in Figure 3. However, even though the velocity field is weaker, the maximum dimensionless temperature is reduced to the half ($\theta_{max} = 0.220$). This behavior must be attributed to an increased conductive heat transfer related to the small separation between the hot and cold walls for the 15° configuration.

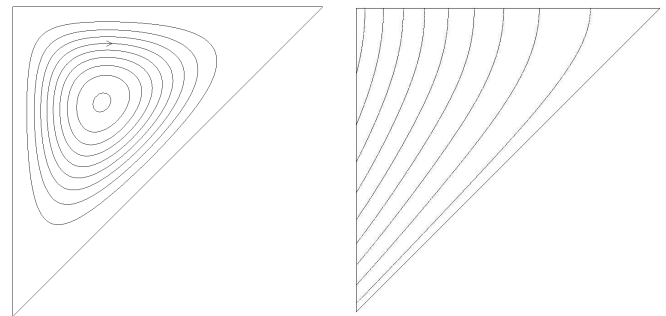


Figure 2 Streamlines and isotherms at $Ra = 10^3$ for $\phi = 45^\circ$
($U_{max} = 2.66 \cdot 10^{-2}$, $\theta_{max} = 0.508$, $\Delta\theta = \theta_{max}/10$).

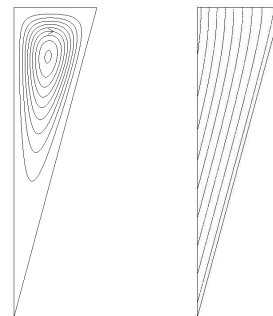


Figure 3 Streamlines and isotherms at $Ra = 10^3$ for $\phi = 15^\circ$
($U_{max} = 2.61 \cdot 10^{-3}$, $\theta_{max} = 0.220$, $\Delta\theta = \theta_{max}/10$).

Figures 4 and 5 illustrate the same results but for a high $Ra = 10^8$. When comparing the streamlines of the cavities for these figures with those in Figures 2 and 3, it is clear that the vortices have moved to the bottom of the cavity. Moreover, now the velocity field function values are increased significantly when compared with the $Ra = 10^3$ case. This increment in the velocity field translates into the fluid flow being dominated by natural convection. As a consequence, we should expect the temperature field to be strongly influenced by the velocity field, as confirmed in Figures 4 and 5. It can be seen that now the isotherms in Figures 4 and 5 are arranged horizontally instead of vertically in the core of the cavity. Since higher velocities are obtained, a more effective heat transfer is expected, which is confirmed by the lower maximum

temperature values obtained along the hot vertical wall. However, it should be noted that now the maximum dimensionless temperature is the same for both cavities.

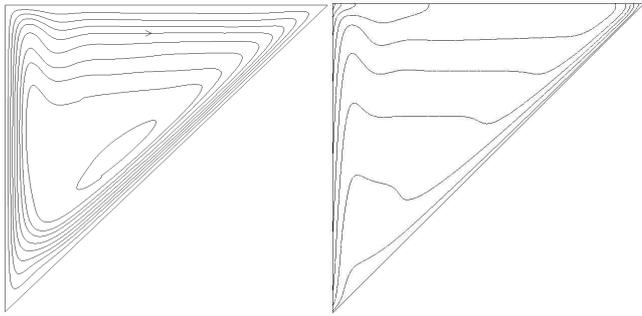


Figure 4 Streamlines and isotherms at $Ra = 10^8$ for $\varphi = 45^\circ$ ($U_{max} = 5.26 \cdot 10^{-2}$, $\theta_{max} = 0.107$, $\Delta\theta = \theta_{max}/10$).

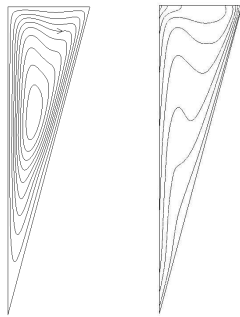


Figure 5 Streamlines and isotherms at $Ra = 10^8$ for $\varphi = 15^\circ$ ($U_{max} = 5.09 \cdot 10^{-2}$, $\theta_{max} = 0.107$, $\Delta\theta = \theta_{max}/10$).

To have a clearer map of the temperature field, the temperature profiles along the hot vertical wall are scrutinized for the cases considered previously. In Figure 6, the dimensionless temperature along the hot wall is plotted for a low $Ra = 10^3$ for the 15° and 45° cavities. It can be seen that dimensionless temperature increases nearly with constant slope, except in the vicinity of the upper edge where the temperature profile changes smoothly to a zero slope value (in harmony with the with the top wall adiabatic boundary condition).

Figure 7 shows the same results but for the high $Ra = 10^8$ case. Two main differences are observed with respect to the results shown in Figure 6. First, it can be seen that the temperature profiles are nearly coincident for the 15° and 45° cavities. The second main difference is that now the temperature profiles present a nearly constant slope along the middle part of the wall and abrupt temperature changes near the edges.

For the purpose of numerically analyzing the heat transfer features of the cavity the Nusselt numbers along the vertical walls are calculated as stated in equation (20)

$$Nu(s) = \frac{q_H \cdot L_H}{k \cdot (T(s) - T_C)} = \frac{1}{\theta(s)} \quad (20)$$

where s represents the distance along the wall, L_H is the wall length, $T(s)$ is the local temperature along the hot wall and $\theta(Y)$ is the local dimensionless temperature along the hot wall.

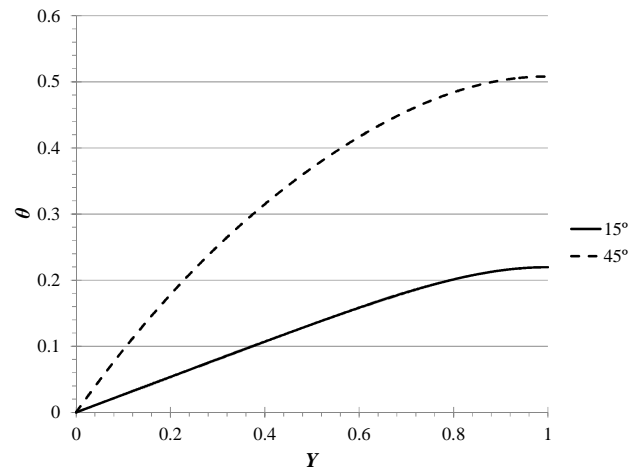


Figure 6 Temperature profile along the heated vertical wall for $Ra = 10^3$ and the two aperture angles (φ) 15° and 45° .

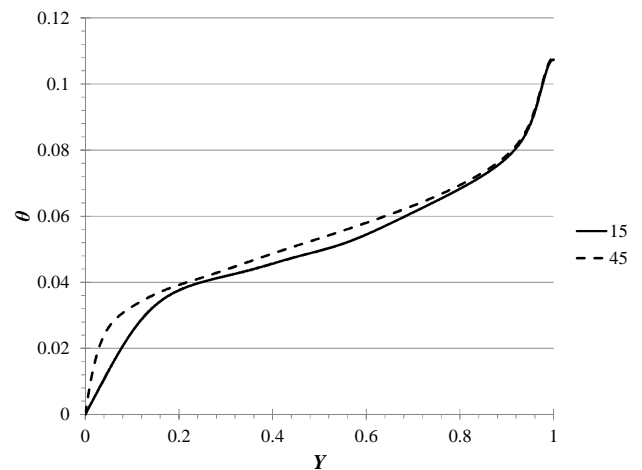


Figure 7 Temperature profile along the heated vertical wall for $Ra = 10^8$ and the two aperture angles (φ) 15° and 45° .

Two different Nusselt numbers are evaluated. The first one is the minimum Nusselt number along the hot wall (Nu_1), which is readily determined from the maximum temperature along the hot vertical wall, as stated in equation (21). The second one is the mean Nusselt number (Nu_2) which is given by equation (22).

$$Nu_1 = \frac{1}{\theta_{max}} \quad (21)$$

$$Nu_2 = \frac{1}{\bar{\theta}(s)} = \frac{L_H}{\int_0^1 \theta(Y) \cdot dY} \quad (22)$$

The minimum Nusselt numbers (Nu_1) are plotted in Figure 8 as function of the Rayleigh number for the three aperture angles analyzed (15°, 30° and 45°). Results show that the Nusselt number grows with the Rayleigh number for all the cases considered. The curves in Figure 8 also reveal that for each aperture angle, Nu_1 is nearly invariant with Ra until a critical Rayleigh number (Ra_{crit}) is attained. The critical Rayleigh number marks the demarcation point between the conduction and convection heat transfer modes. Figure 8 also reveals that the critical Rayleigh number increases when the aperture angle diminishes.

Comparing the results for the three aperture angles reflects that when the aperture angle is reduced from 45° to 15°, the minimum Nusselt number (Nu_1) increases remarkably in the low Ra range. However, for values of the Rayleigh number higher than the critical one, the Nu_1 curves for the three cavities tend to converge into a single one. This means, that from the view of controlling the superficial temperatures of the wall (controlling the maximum or critical temperature) the three cavities perform similar once the Rayleigh value is sufficiently high enough to guarantee that the convective heat transfer mode is active.

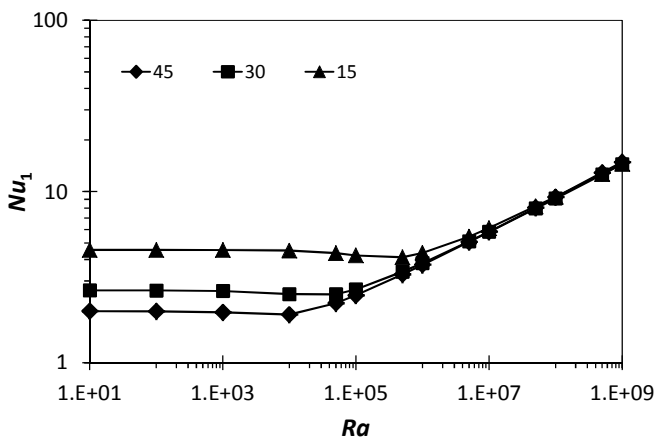


Figure 8 Variation of the minimum Nusselt number with the Rayleigh number for the three aperture angles 15°, 30° and 45°.

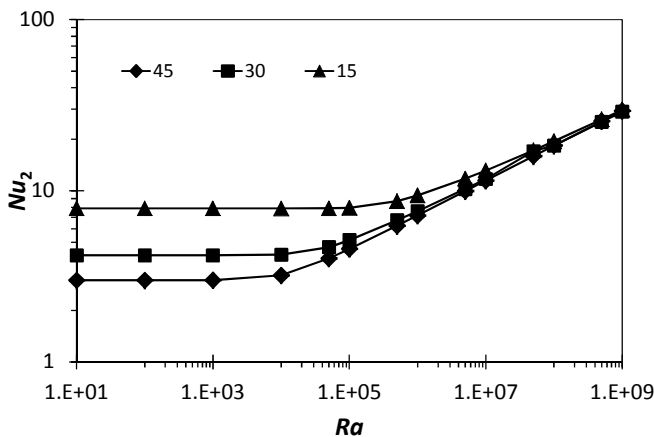


Figure 9 Variation of the mean Nusselt number with the Rayleigh number for the three aperture angles 15°, 30° and 45°.

Figure 9 shows the same results but for the mean Nusselt number (Nu_2). An analysis of the results in Figure 9 leads to similar conclusions that those obtained for Figure 8. Since Nu_2 is based on the hot wall average temperature rather than on the maximum or critical temperature, the values of Nu_2 are higher than Nu_1 by a factor between 1.5 and 2.

CONCLUSIONS

In this paper the problem natural convection has been analyzed in a right-angled triangular cavity filled with air. The analysis was performed for height-based Rayleigh numbers that range from a low $Ra = 0$ (pure conduction) to a high $Ra = 10^9$ and for the three aperture angles of 45°, 30° and 15°. The numerical computations were channeled through the determination of the minimum and mean Nusselt numbers along the hot vertical wall, which are based on the maximum and mean temperatures along the hot vertical wall, respectively.

The following major conclusions are drawn from the analysis of the numerical results.

1. A critical Rayleigh number exists that marks the threshold between the conduction mode and the natural convection mode. The critical Rayleigh number decreases for higher aperture angles.

2. For all the configurations, the minimum and mean Nusselt numbers at the hot wall increases with increments in the Rayleigh number.

3. For low Rayleigh numbers the thermal performance increases for lower aperture angles. This behavior must be attributed to an increased conductive heat transfer related to the small separation between the hot and cold walls.

4. In contrast, for high Rayleigh numbers the thermal performance is merely equal for the three aperture angles studied. Then, the same value of the maximum or critical temperature along the hot vertical wall is obtained.

REFERENCES

- [1] Ostrach S., Natural convection in enclosures, *J. Heat Transfer*, Vol. 110, 1988, pp. 1175-1190.
- [2] Raithby G.D., and Hollands K.G.T., Natural convection, in: Rohsenow W.M., Harnett J.P., and Cho Y.I. (Eds.), *Handbook of Heat Transfer*, 3rd ed., Mc Graw-Hill, New York, 1998, Chapter 4.
- [3] Jaluria Y., Natural convection, in: Bejan A., and Kraus A.D. (Eds.), *Heat Transfer Handbook*, Wiley, New York, 2003, Chapter 7.
- [4] Fusegi T., Hyun J.M., and Kuwahara K., Natural convection in a differentially heated square cavity with internal heat generation, *Numer. Heat Transfer A*, Vol. 21, 1992, pp. 215-229.
- [5] Markatos N.C., and Pericleous K.A., Laminar and turbulent natural convection in an enclosed cavity, *Int. J. Heat Mass Transfer*, Vol. 27, 1984, pp. 755-772.
- [6] Holtzman G.A., Hill R.W., and Ball K.S., Laminar natural convection in isosceles triangular enclosures heated from below and symmetrically cooled from above, *J. Heat Transfer*, Vol. 122, 2000, pp. 485-491.
- [7] Rahman M., and Sharif M.A.R., Numerical study of laminar natural convection in inclined rectangular enclosures of various aspect ratios, *Numer. Heat Transfer A*, Vol. 44, 2003, pp. 355-373.

- [8] Heindel T.J., Ramadhyani S., and Incropera F.P., Assessment of turbulence models for natural convection in an enclosure, *Numer. Heat Transfer B*, Vol. 26, 1994, pp. 147-172.
- [9] Del Campo E.M., Sen M., and Ramos E., Analysis of laminar convection in a triangular enclosure, *Numer. Heat Transfer A*, Vol. 13, 1988, pp. 353-372.
- [10] Simons R.E., Antonnetti V.W., Nakayawa W., and Oktay S., Heat transfer in electronic packages, in: Tummala R. R., Rymaszewski E.J., and Klopfenstein A.G. (Eds.), *Microelectronics Packaging Handbook*, 2nd ed., Chapman and Hall, New York, 1997, pp. 1-315 to 1-403.
- [11] Bar-Cohen A., Watwe A.A., and Prasher R.S., Heat transfer in electronic equipment, in: Bejan, A., and Kraus A.D. (Eds.), *Heat Transfer Handbook*, Wiley, New York, 2003, Chapter 13.
- [12] COMSOL, 2008. COMSOL, Inc., COMSOL Multiphysics User's Guide, Version 3.5, Burlington, MA.
- [13] Davis T.A., Algorithm 832: UMFPACK V4.3—An Unsymmetric-Pattern Multifrontal Method, *ACM Transactions on Mathematical Software*, Vol. 30, no. 2, 2004, pp. 196-199.
- [14] Lemmon E.W., Huber M.L., McLinden M.O., NIST Standard Reference Database 23: Reference Fluid Thermodynamic and Transport Properties-REFPROP, Version 9.0, National Institute of Standards and Technology, Standard Reference Data Program, Gaithersburg, 2010.